Tipping the ENSO into a permanent El Niño can trigger state transitions in global terrestrial ecosystems

Mateo Duque-Villegas[1], Juan F. Salazar[1], and Angela M. Rendón[1]

[1]GIGA, Escuela Ambiental, Facultad de Ingeniería, Universidad de Antioquia, Medellín, Colombia

Correspondence: Juan F. Salazar (juan.salazar@udea.edu.co)

Abstract. Some large-scale components of the Earth's climate system have been identified as policy-relevant "tipping elements", meaning that anthropogenic forcing and perturbations may push them across a tipping point threshold, with potential global scale impact on ecosystems and concomitant environmental and social phenomena. A pronounced change in the amplitude and/or frequency of the El Niño–Southern Oscillation (ENSO) is among such tipping elements. Here we use the Planet Simulator (PlaSim), an Earth system model of intermediate complexity, to investigate the potential impact on global climate and terrestrial ecosystems of shifting the current dynamics of the ENSO into a permanent El Niño. When forced with sea surface temperature (SST) derived from observations, the PlaSim model yields a realistic representation of large-scale climatological patterns, including realistic estimates of the global energy and water balances, and gross primary production. In a permanent El Niño state, we found significant differences in the global distribution of water and energy fluxes, and associated impacts on gross primary production, indicating that vegetation productivity decreases in the tropics whereas it increases in temperate and boreal regions. We identify regions in which these El Niño-induced changes are consistent with potential state transitions in global terrestrial ecosystems, including potential dieback of the Amazon rainforest, southward expansion of the Sahel, and further aridification of Australia.

1 Introduction

Earth's current climatology can be considered a steady state of a non-equilibrium system (Kleidon, 2010) in which constant influx of solar radiation and internal feedback mechanisms stall equilibrium, so that properties of the climate system can remain relatively close to mean values. However, it is becoming increasingly clear that the Earth's climate system as a whole, as well as some of its large-scale components or subsystems, have tipping points (i.e. critical thresholds in forcing and/or a feature of the system) at which the system shifts from one state (e.g. current climate) to another (e.g. future climate) (Lenton et al., 2008; Scheffer et al., 2009). Perturbations related to human-induced climate change could push several Earth's subsystems past a tipping point (Lenton, 2011; Barnosky et al., 2012), potentially changing the modes of natural climatic variability (Cai et al., 2015).

Lenton et al. (2008) identified several *tipping elements* in the Earth's climate system. A tipping element is a large-scale component of the Earth system that may pass over a tipping point with the potential to alter global climate. A pronounced change in the amplitude and/or frequency of the El Niño–Southern Oscillation (ENSO), including its shifting into a permanent

El Niño state, is among the policy-relevant tipping elements identified by Lenton et al. (2008). Although there is no definitive evidence at present for specific changes in ENSO behaviour in response to climate change (McPhaden et al., 2006; Cai et al., 2015), global climate modeling studies do indicate the possibility of ENSO intensification during the 21st century due to anthropogenic forcing (Timmermann et al., 1999; Guilyardi, 2006). Greenhouse warming in climate projections can lead to

5 more frequent El Niño events, because it diminishes temperature gradients in the eastern equatorial Pacific Ocean, which facilitate the changes in convection zones that are observed during this phenomenom (Cai et al., 2014; Latif et al., 2015).

Through atmospheric teleconnections, ENSO exerts strong effects on manifold environmental and social systems at global to regional scales (Diaz and Markgraf, 2000; Cai et al., 2015; Yeh et al., 2018; McPhaden et al., 2006), including major implications for the functioning of terrestrial ecosystems (Holmgren et al., 2001). For instance in Amazonia, temperature and

10 precipitation changes associated with ENSO have been found to alter the net carbon flux to the atmosphere and seasonal inundation of floodplains (Foley et al., 2002). Moreover, El Niño-induced droughts in Amazonia increase the likelihood of forest fires that modify landscape features and have top-down effects that damage not only vegetation but also faunal populations (Alencar et al., 2006). Similarly, in Australia's drylands, ENSO is a modulator of biomass removal through fires and grazing (Holmgren et al., 2006). Such land-use impacts are particularly important in places where the population largely depends on

15 agriculture, such as south-eastern Africa, where ENSO also affects rainfall patterns (Indeje et al., 2000). Therefore, and despite the inherent uncertainty of climate change projections, the potential impact of shifting the state of the ENSO is of global concern (Lenton et al., 2008; Cai et al., 2014). Advancing the quantitative understanding of the range of expected physical climate changes (let alone tipping events) and their potential impact on different sectors and/or regions is crucial for decision-making related to global change (Lenton and Ciscar, 2013; Zebiak et al., 2015).

20 Here we used the Planet Simulator (PlaSim; Fraedrich et al., 2005a, b) to investigate the potential impact on global climate of shifting the dynamics of the ENSO into a permanent El Niño state, and examine the potential consequences of this tipping event on global terrestrial ecosystems. Our aim was to see what Earth's climate could be if the climatology of SST were that observed during a warm phase of ENSO. Thus we simulated a control scenario and compared it to current climate using observations derived data sets, in order to understand the model's limitations. Then we set up a permanent El Niño experiment

25 and compared it to a control simulation, focusing on the impacts on water deficit and terrestrial ecosystems.

2 Model description

PlaSim is a climate model of intermediate complexity. This type of models are well-suited for our goals because of their ability to parsimoniously simulate feedbacks between many components of the climate system over long-term simulation ensembles covering a global domain (Claussen et al., 2002). The dynamical core of PlaSim is based on PUMA (Fraedrich et al., 2005c), an

30 atmospheric general circulation model that solves the moist primitive equations representing the conservation of momentum, mass and energy in the Earth's atmosphere, using a vertical σ coordinate and the spectral transform method with triangular truncation over a sphere (Orszag, 1970; Hoskins and Simmons, 1975). Unresolved sub-grid scale processes such as radiation,

moist and dry convection, large-scale precipitation, surface fluxes and vertical and horizontal diffusion are parameterized (Lunkeit et al., 2011).

The atmospheric model is coupled to a 5-layer land surface model that includes parameterizations for soil temperature, snow cover and a bucket-type runoff transport scheme (Sausen et al., 1994). A dynamic vegetation model (SimBA) included

5 in PlaSim allows to represent vegetation-atmosphere feedbacks through climate-induced changes in large-scale surface parameters such as albedo, roughness and water holding capacity (Kleidon, 2006). The ocean can be represented through prescribed climatological values of SST or using dynamical models (Fraedrich, 2012; Semtner Jr, 1976). For more details about the model description we refer the reader to Fraedrich et al. (2005a) and Lunkeit et al. (2011).

PlaSim has been successfully used to study the evolution of the Earth's climate system under different physical scenarios

10 and forcings. One of the first applications of PlaSim was to estimate the maximum possible influence of vegetation on the global climate through simulation of two extreme scenarios: "green planet" and "desert world" (Fraedrich et al., 2005b). More recent applications have studied the planetary climate system response to, for instance, vegetation-atmosphere feedbacks (Dekker et al., 2010; Bathiany et al., 2012), large-scale changes in orography (Garreaud et al., 2010; Schmittner et al., 2011), and variations in astronomical forcings (Boschi et al., 2013; Linsenmeier et al., 2015). The model has also been used for

15 paleoclimate studies (Henrot et al., 2009) and snowball Earth experiments (Spiegl et al., 2015; Lucarini et al., 2013). Some of these studies have also explored the existence of alternative equilibrium states of the planetary climate system, as well as the mechanisms behind potential state transitions (Dekker et al., 2010; Bathiany et al., 2012; Boschi et al., 2013; Linsenmeier et al., 2015).

3 Experimental setup

20 For all simulations, PlaSim was implemented with a spectral horizontal resolution of T21 (about 5.6° on a Gaussian grid) and 10 non-equally spaced σ vertical levels. Though relatively coarse, this resolution allows a realistic representation of large-scale atmospheric circulation (Linsenmeier et al., 2015) and baroclinic structures that are important in the energy transport polewards in a slowly rotating and phase locked planet like the Earth (Lucarini et al., 2013). All simulations were integrated for 500 years at 40 minutes time steps, with model output being stored as daily averages. This long term simulation allows the model to

25 approach an equilibrium state (Lucarini et al., 2017), which we characterized using the last 30 years of each simulation. The dynamic vegetation model SimBA was used to allow variations in terrestrial ecosystems. The solar constant and atmospheric CO_2 were always set at present-day values of $1365 \, \mathrm{W \, m^{-2}}$ and 360 ppmv, respectively. All other model physical constants, planetary values and tuning parameters were kept at their default setting (Fraedrich et al., 2005b).

The ocean was represented through prescribed SST values that were used to define two scenarios: ConTroL (CTL) and

30 Permanent El Niño (PEN). Difference between scenarios is entirely determined by differences in the prescribed SST annual cycle (Figs. 1 and S1). Due to the inherent chaotic nature of atmospheric dynamics, each scenario was studied using an equally weighted ensemble of three simulations with different initial conditions, which were varied through a random noise disturbance
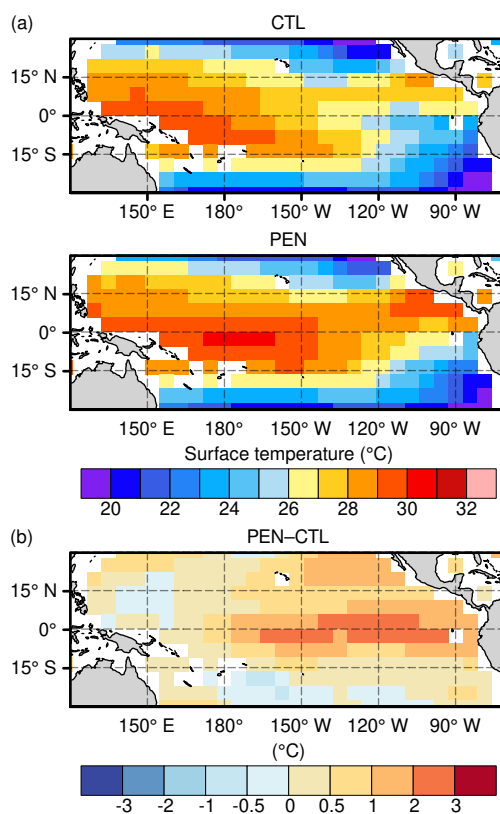
Figure 1. Prescribed SST climatology annual mean in the equatorial Pacific Ocean region for CTL and PEN simulations (a), and their absolute difference (b).

in the surface pressure field (e.g. Kunz et al., 2009). Average results from different simulations were compared using a Student's *t*-test at a significance level of $\alpha = 0.05$ and 30 degrees of freedom (corresponding to a 30-year simulation period).

3.1 Control scenario and model evaluation

The CTL scenario is based on present-day climatology and therefore was first used to assess the model's ability to realistically
5 represent the Earth's climate system, and then used as reference for comparing with the PEN scenario. The CTL scenario is characterized by a climatological annual cycle of SST values obtained from the second phase of the Atmospheric Model Inter-comparison Project (AMIP II) for the period 1979–2010 (Hurrell et al., 2008). Regridding to model resolution and adjusting the least possible temperature to be 271.38 K was done following recommendations by Taylor et al. (2000).

Observational gridded data sets used to compare with the model results for the CTL scenario are: 1987–2016 monthly values
10 of precipitation from the Global Precipitation Climatology Project (GPCP; Adler et al., 2003); 1988–2017 monthly values of near surface air temperature from the HadCRUT4 data set (Morice et al., 2012); 1979–2004 monthly values of mean sea level pressure from the HadSLP2 data set (Allan and Ansell, 2006); 2000–2015 monthly values of gross primary production (GPP)

from the MODIS product MOD17A2 (Zhao et al., 2005); and 1987–2016 monthly values of free air temperature, as well as
zonal and meridional winds at different pressure levels (1000–50 hPa) from the European Centre for Medium-range Weather
Forecasts (ECMWF) Interim reanalysis (ERA-Interim; Dee et al., 2011). The global energy and water balances produced by
PlaSim were compared with estimates based on ERA-Interim and those reported by Trenberth et al. (2011). More details about
5   all data sets used in this work are shown in Tables S1 and S2 in the supplementary material.

3.2   Permanent El Niño

In this scenario the prescribed climatological annual cycle of SST was replaced with the annual cycle of El Niño occurred
between 2015 and 2016, using June, 2015 to May, 2016 SST monthly values from the AMIP II data set. This is the strongest
El Niño recorded so far, surpassing strong events from last century: 1982–1983 and 1997–1998 (Jiménez-Muñoz et al., 2016).
10   The bottom panel (or b) in Fig. 1 depicts the annual mean differences between the PEN and CTL scenarios for the equatorial
Pacific region. It can be seen that this El Niño event depicted well the first main mode of spatio-temporal variability of SST
anomalies (the mature phase of ENSO) and did not exhibit the El Niño Modoki second main mode (Ashok et al., 2007). The
PEN climatology has a global annual warm bias of +0.4 °C, with both boreal winter (DJF) and autumn (SON) seasons having
the largest positive deviations (see Fig. S1 in supplementary material). The warm bias is greater specifically in the equatorial
15   Pacific Ocean, where it reaches an annual mean value of +0.8 °C.

3.3   Climatological water deficit estimation

In this study we focus on the consequences that such a PEN climate scenario could have for terrestrial ecosystems. We used
the maximum climatological water deficit (MCWD) as defined by Aragao et al. (2007), which is an indicator of accumulated
water stress during dry seasons that has been linked to ecosystem degradation via hydraulic failure in plants (Leitold et al.,
20   2018), fires (Brando et al., 2014) and deforestation (Costa and Pires, 2010). We followed an approach similar to Malhi et al.
(2009), who plot MCWD versus mean annual precipitation (MAP) to study the possibility of land cover transitions under
climate change projections in the Amazon rainforest. Malhi et al. (2009) found that most savannah biomes in Amazonia (i.e.
Cerrado), had rainfall rates below 1500 mm year^{-1} and accumulated water deficits more negative than -300 mm. Unlike Malhi
et al. (2009), our aim was global and, therefore, in order to be able to calculate MCWD, we could not use a single fixed ET
25   value for the full extent of our domain. Instead we used annual mean ET for every gridpoint from the CTL scenario as a proxy
of expected ET with current land cover. These reference values (Fig. S9) agree with the approximation used by Malhi et al.
(2009) of 100 mm month^{-1} of average ET rate for the Amazonia. Likewise, we assumed soil saturation at the wettest time of
the year and set the cumulative water deficit to zero at this month (Fig. S10).

Additionally, the effects that a PEN scenario could have on terrestrial ecosystems are easier to observe when MAP and
30   MCWD are merged together. Thus to present our results more clearly, we created a composite map that shows where both
quantities changed considerably. We defined the 10 % of the CTL value as a threshold to identify places where differences
between scenarios were the largest. In this way what we mean by "much more/less" or "much greater", is that this difference

exceeds the threshold. Otherwise, even though both MAP and MCWD changed for a particular gridpoint, this change was not as pronounced.

4 Results

Altogether, the PlaSim CTL simulation realistically represents the broadscale patterns seen in observational data of present-day
5 climate. In spite of PlaSim's simplicity and coarse resolution of the simulations, the model produces a realistic representation of the current climatological state of the Earth's climate system. Our results generally agree with previous studies showing that PlaSim is able to simulate many dominant features of the present-day climate (e.g. Garreaud et al., 2010; Lucarini et al., 2017).

4.1 Control climate

A comparison between PlaSim results for the CTL scenario and estimates from ERA-Interim and Trenberth, Fasullo, and
10 Mackaro (2011, henceforth TFM11) shows that simulations produce realistic estimates of the global energy and water budgets (Fig. 2). The magnitude of the net energy imbalance at the top of the atmosphere, TOA, (i.e. the difference Δ between incoming and outgoing radiation) is lower for PlaSim ($\Delta = -0.8$ W m^{-2}) than it is for ERA-Interim ($\Delta = -1.4$ W m^{-2}) and TFM11 ($\Delta = +0.9$ W m^{-2}). Previous studies have reported that PlaSim's energy imbalance is closer to zero than it is for many state-of-the-art climate models (Lucarini et al., 2010). Differences between PlaSim and observations indicate that the model
15 overestimates the outgoing solar radiation at TOA, as a result of more solar radiation being reflected both at the surface and atmosphere, and less solar radiation being absorbed by the atmosphere. However, the model's estimate of solar radiation absorbed at the surface falls between those of ERA-Interim and TFM11. The surface energy balance in the model shows realistic estimates of thermal, latent heat and sensible heat fluxes, with a slightly overestimated Bowen ratio (SH/LH) of 0.23 as compared to 0.21 in both ERA-Interim and TFM11. These biases in the surface fluxes are likely to be related to prescribed
20 values of aerodynamic roughness length (Yang et al., 2002), which has also been related to ERA-Interim biases (Zhou and Wang, 2016). The model's representation of the greenhouse effect through the estimate of thermal energy emitted by the atmosphere falls also within estimates from ERA-Interim and TFM11.

As for the water budget, PlaSim produces a realistic distribution of water among ocean, land and atmosphere, preserving key hydrological cycle characteristics: greater evaporation than precipitation over the oceans and greater precipitation than
25 evapotranspiration over continental areas (Fig. 2b). As compared to TFM11, atmospheric transport from ocean to land, as well as continental runoff, are underestimated both in PlaSim and ERA-Interim, but unlike the reanalysis, the water balance for the model shows conservation. This is partly because the model values are not affected by any assimilation scheme as is the reanalysis (Seager and Henderson, 2013). Overall, PlaSim estimates of global water fluxes fall within the uncertainty ranges proposed by Trenberth et al. (2011) for ERA-Interim and other reanalyses.
30 There are statistically significant differences between PlaSim and observational data in the global annual mean distribution of near surface air temperature (Fig. 3a,b), precipitation (Fig. 3c,d), GPP (Fig. 3e,f) and mean sea level pressure (Fig. 3g,h). However, these biases are within typical ranges obtained for more comprehensive state-of-the-art climate models (Stevens et al.,
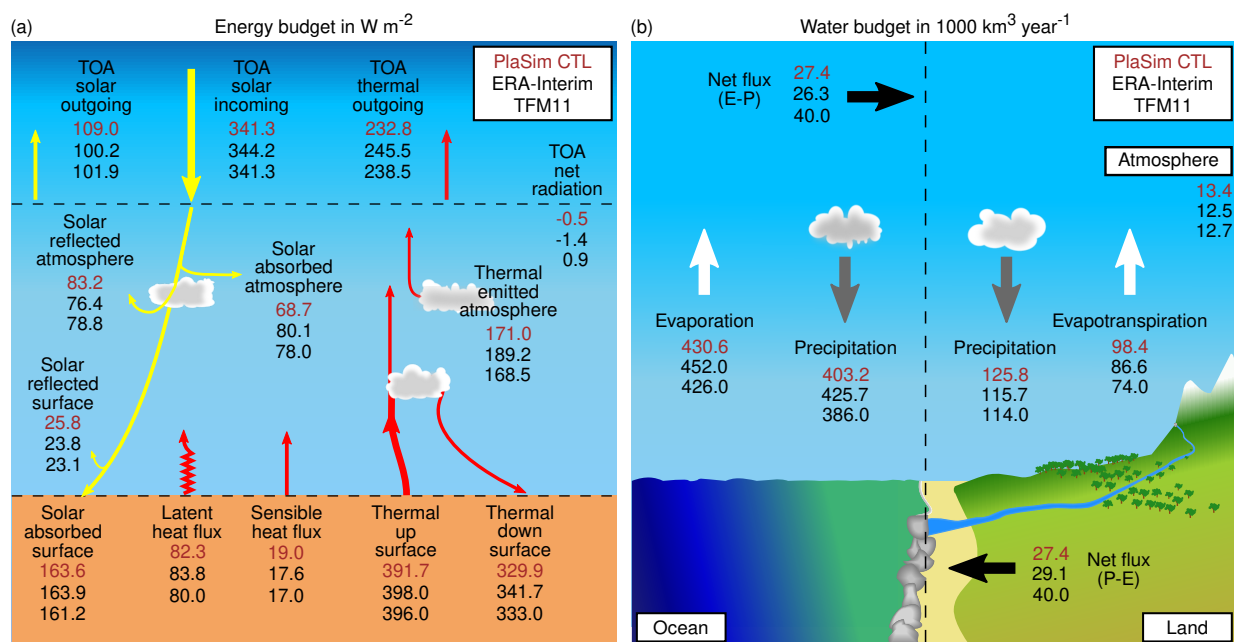
Figure 2. Global average annual mean energy (a) and water budget (b) for the CTL simulation compared with ERA-Interim and Trenberth et al. (2011).

2013), and cannot be entirely attributed to model deficiencies because of uncertainties in the observational data sets themselves (e.g. Prein and Gobiet, 2017). Importantly, large-scale spatial patterns of near surface air temperature, precipitation, GPP and mean sea level pressure (Fig. 3), as well as their seasonality (Figs. S2–5), are realistically represented by PlaSim.

Differences between PlaSim results and HadCRUT4 (Fig. 3b) indicate that the model exhibits a global average cold bias

5   of about -0.2 °C. This global bias arises from an average warm bias of +1.6 °C over continental areas and an average cold bias of -1.0 °C over the oceans. The global average annual mean temperature in the CTL simulation (14.1 °C) is similar to that from observations (14.4 °C). Seasonal variations of temperature are realistically simulated too (Fig. S2). Some of the largest temperature biases occur on land near polar regions, especially in Greenland and Antarctica, and regions with complex terrain such as the Himalayas mountain range in Asia. Biases over complex terrain are related to known limitations even in

10   state-of-the-art climate models, partly because the orography representation has to be smoothed to keep dynamical stability (Flato et al., 2013). A warm bias in western Africa and Australia and a slight cold bias in the Sahara desert and Amazonia are also observed. Strongest biases take place in boreal summer (JJA) and autumn (SON) seasons, when the global average biases on land are +3.1 °C and +2.6 °C respectively. Over the oceans, temperatures are colder than observations year-round but the average bias has a maximum of -1.2 °C in boreal winter (DJF).

15   Annual mean daily precipitation from the CTL simulation is depicted in Fig. 3c. The large-scale patterns exhibited in GPCP are present: the equatorial maximum in the Inter-Tropical Convergence Zone (ITCZ), midlatitudes peaks of synoptic-scale weather systems and low precipitation rates in the polar regions. There are high precipitation rates over the western equatorial
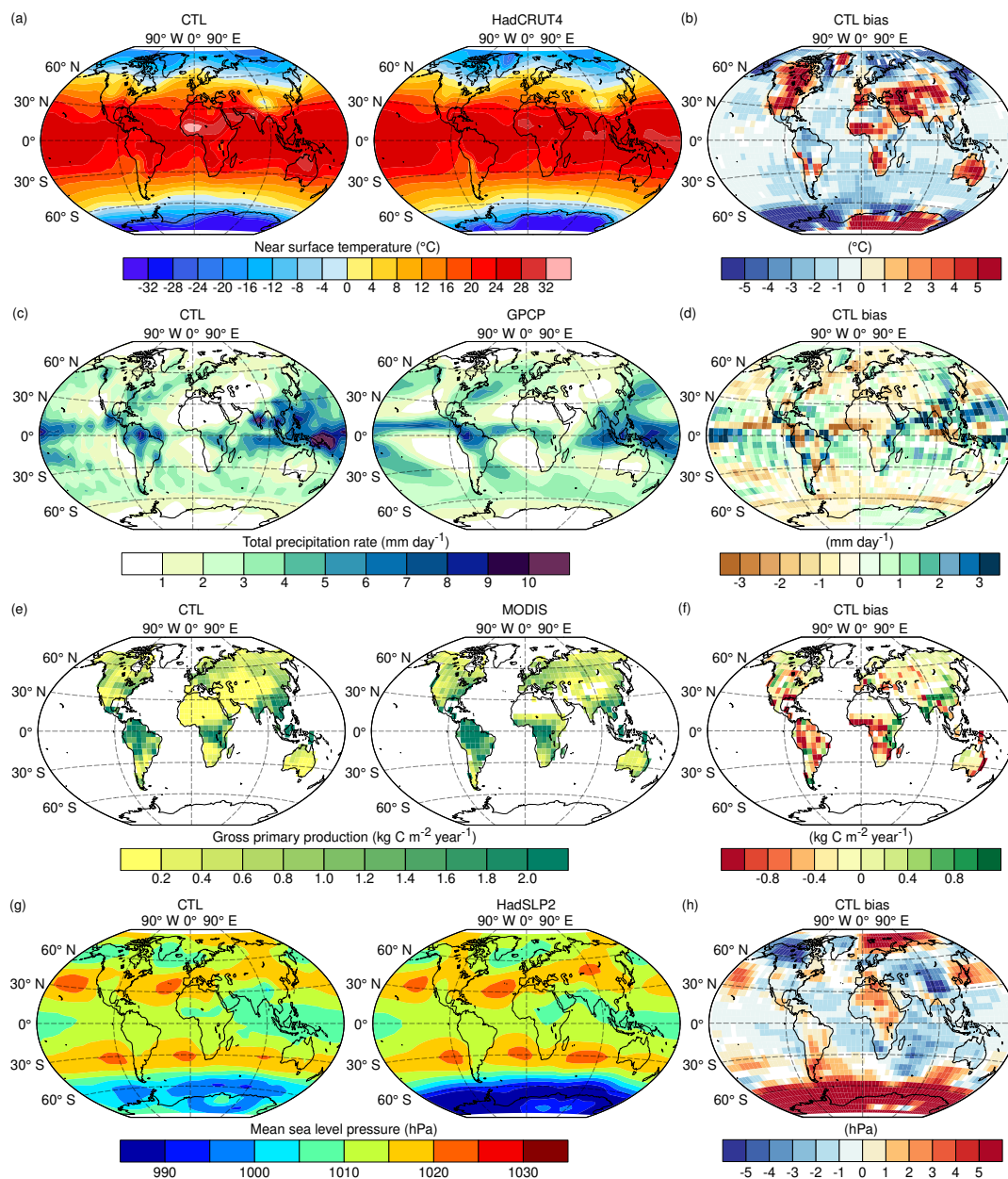
Figure 3. Annual mean results for the CTL simulation compared with observational data: near surface temperature in CTL and HadCRUT4 (a) and its bias (b); total precipitation in CTL and GPCP (c) and its bias (d); GPP in CTL and MODIS (e) and its bias (f); and mean sea level pressure in CTL and HadSLP2 (g) and its bias (h). In the bias panels, white depicts gridpoints with statistically non-significant difference ($\alpha = 0.05$).

Pacific and the western hemisphere warm pools. The PlaSim global average annual mean precipitation rate reaches 2.8 mm per

day, whereas for observational data it is 2.7 mm per day. Concerning seasonal variation (Fig. S3), tropical precipitation shows latitudinal displacement and has maximum peaks in south-eastern Asia in the boreal winter (DJF) and summer (JJA) seasons. In northern South America the maximum of precipitation crosses the equator twice a year, unlike over the eastern Pacific where the ITCZ stays north of the equator for all seasons. PlaSim also displays the double ITCZ band that has been described for
5   other global climate models (Lin, 2007), especially during the boreal spring season (MAM).

Figure 3e shows the dynamic vegetation results for GPP in continental areas. Observational data from MODIS contains missing and null values in desert areas in Africa, in the middle East, as well as in Greenland, Antarctica and near the Himalayas. Global average annual mean for the CTL simulation reaches $0.8\,\mathrm{kg\,C\,m^{-2}}$ per year, whereas for MODIS data it is $1.0\,\mathrm{kg\,C\,m^{-2}}$ per year. Although large deviations with respect to MODIS can be seen in Fig. 3f, these are similar to those reported in other
10   modelling studies and could be related to the climate data sets used as input in the simulations (Ardö, 2015; Wu et al., 2018). Differences between this model and other data sets (whether derived from observations or not) occur because parameterization schemes to obtain GPP indirectly from climate variables are different. Nevertheless, the model shows a realistic estimate of the GPP distribution with high productivity near the equator and low productivity elsewhere. Also the location of the subtropical deserts is consistent with observations. Furthermore, the model is able to represent seasonal changes in primary productivity
15   (Fig. S4). There is a year-round high productivity around the equator, whereas for the northern and southern hemispheres it is maximum in their respective summer season and it is minimum in their respective winter season.

When compared with observations, PlaSim also displays a very similar annual mean pattern of high and low pressure cells in the subtropics (Fig. 3g). The largest differences are seen in Antarctica, where the model overestimates sea level pressure (Fig. 3h). Seasonally, the model is also able to represent the appearance of semi-permanent pressure systems throughout the
20   year (Fig. S5). For instance, in the northern hemisphere, the Aleutian and Icelandic lows and the Pacific, Azores and Siberian highs are seen in winter, whereas only the Pacific and Bermuda highs are seen in the summer season.

Regarding general circulation, the temperature gradient in the atmosphere for the CTL simulation has a very similar structure as the one from ERA-Interim reanalysis (Fig. 4a,b). Differences are relatively small below 500 hPa and away from the poles. Strongest biases are found around 200 hPa. In the upper troposphere, the model is much warmer in the tropics and much cooler
25   near the northern hemisphere pole. This behaviour is common to most general circulation models, which have difficulties parameterizing moist thermodynamic processes (Santer et al., 2017). Convective heating is overestimated in the Kuo-type convection scheme implemented in PlaSim (Arakawa, 2004).

The distribution of temperature is closely related to the zonal wind velocity (Fig. 4c,d). The location of the sub-tropical jet streams in the CTL simulation is in agreement with ERA-Interim, with the zonal wind speeds of the jet streams being higher
30   in PlaSim. As with temperature, main differences are found in the upper troposphere and the lower stratosphere above 200 hPa. This is a known problem with some general circulation models that display too fast zonal jet streams due to a coarse representation of the planet's orography and simple representation of the low-level drag (Pithan et al., 2016). The trade winds in PlaSim prevail around the equator, but are slower than in the reanalysis below 300 hPa, and faster above. As compared to ERA-Interim, zonal wind speed is underestimated eastward in PlaSim at 60° S at all pressure levels.
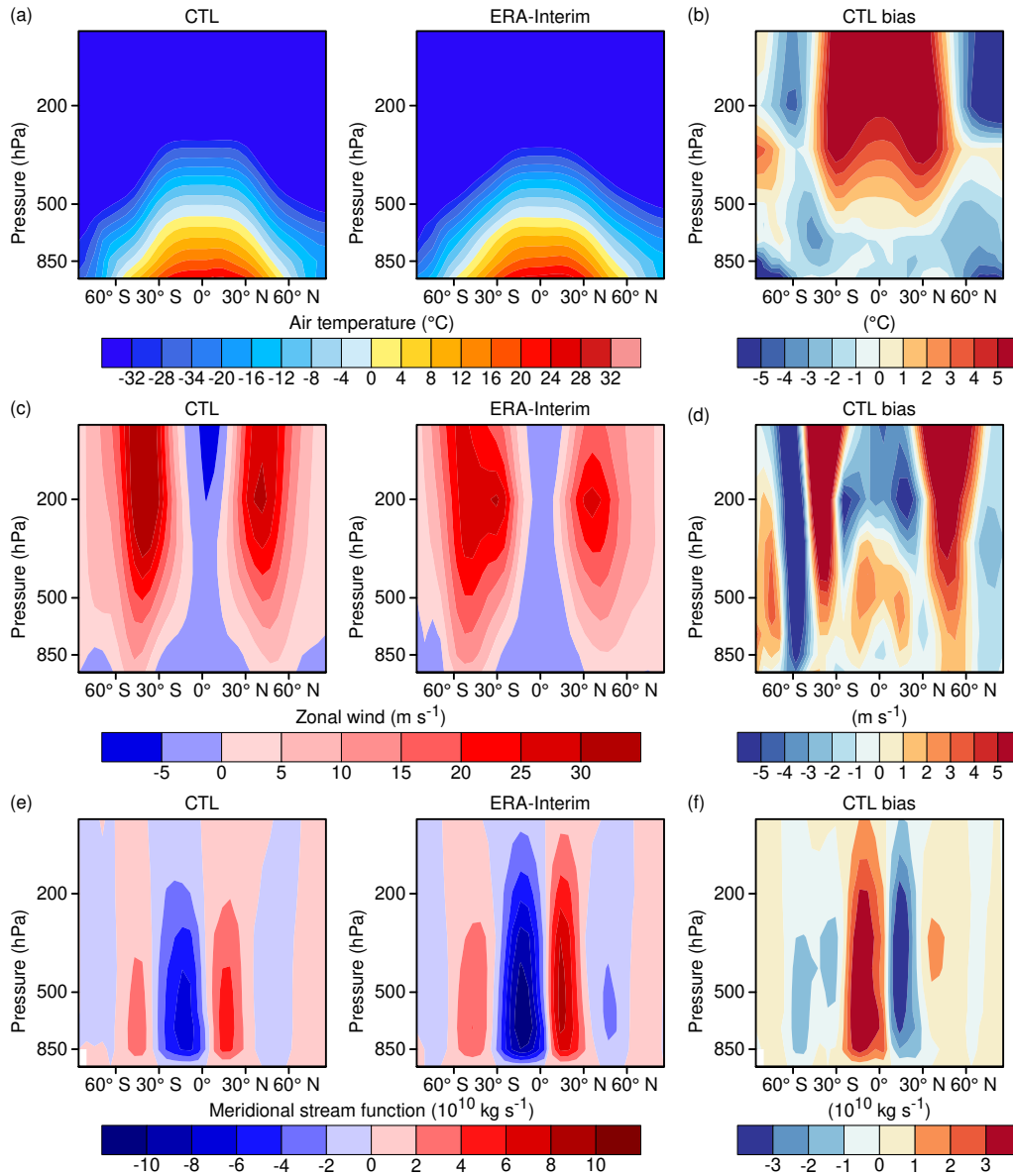
Figure 4. Zonal average annual means results for the CTL simulation compared with ERA-Interim at different pressure levels for: (a) air temperature and (b) its model bias; (c) zonal wind and (d) its model bias; and (e) meridional stream function and (f) its model bias.

PlaSim adequately simulates the thermally induced Hadley cell and its displacement across the equator for the annual mean (Fig. 4e,f), with clockwise rotation when in the southern hemisphere and counter-clockwise in the northern. As described for observations, when in the southern hemisphere, the cell is stronger. Similarly, the indirect Ferrell cell can be seen moving in the opposite direction as the former (different colour in Fig. S7e,f). Differences in the stream function occur for the Hadley

5   cell at both hemispheres, which is slower and shorter in PlaSim. Because of this, the indirect Ferrell cell is also smaller and
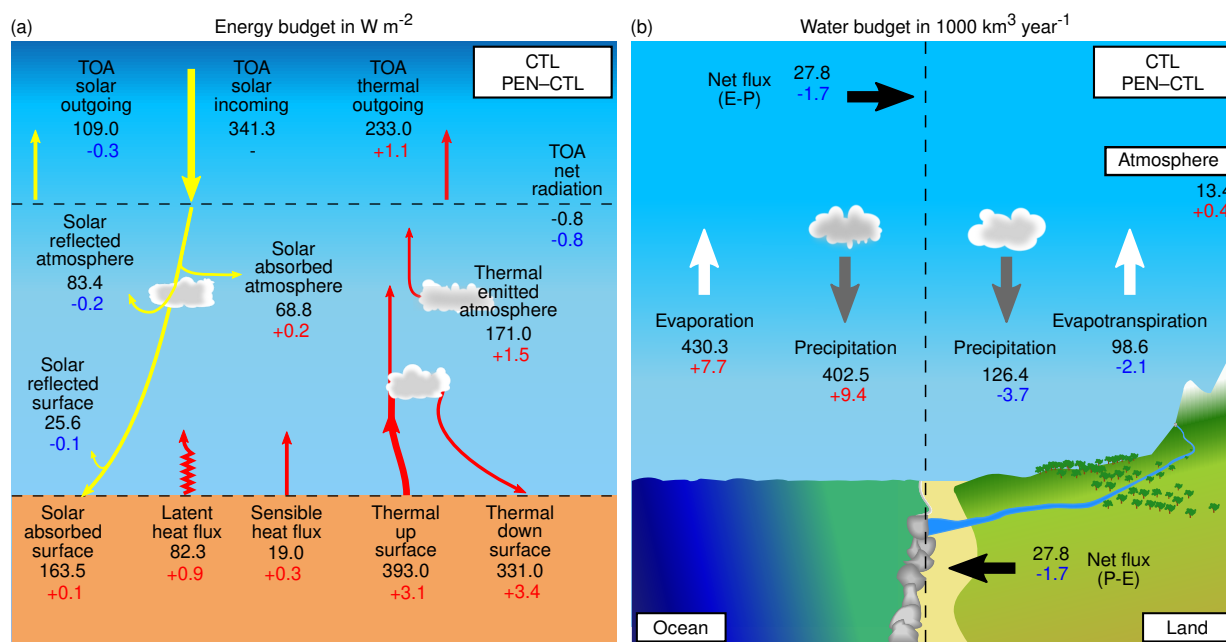
Figure 5. Global average annual mean (a) energy and (b) water budget for the PEN simulation compared with the CTL simulation.

is almost absent when in the northern hemisphere. Polar cells are present but not visible in any of these figures because of the chosen contour levels.

4.2 Permanent El Niño climate

Much warmer than usual equatorial Pacific Ocean temperatures, as depicted in the PEN scenario, lead to statistically significant

5 changes in the global energy and water budgets (Fig. 5a). For the energy budget a warmer ocean surface means higher long-wave radiation being emitted, as seen in the heat fluxes and the thermal upward radiation. Warmer temperatures diminish surface snow and sea ice formation, which is followed by a low planetary effective albedo and, therefore, less solar incoming radiation is reflected. At the same time the atmosphere becomes warmer and thermal emission increases. Ultimately this leads to less incoming solar radiation being reflected, and more thermal radiation being emitted back to space. These two processes

10 do not balance each other in the model and, therefore, the net imbalance at TOA becomes more negative than in the CTL simulation. Overall the PEN scenario shows much warmer surface and atmosphere than the CTL.

According to PEN simulation outputs, water is redistributed throughout the world (Fig. 5b). A warmer atmosphere stores more water, but the net transport of water from the ocean to land is reduced. This may be explained by changes in wind patterns over the Pacific Ocean, linked to the Walker circulation, which keep most water vapour above the ocean surface, as is typical

15 during El Niño conditions (Diaz and Markgraf, 2000). Consistently, evaporation and precipitation increase over the ocean while they decrease on land.
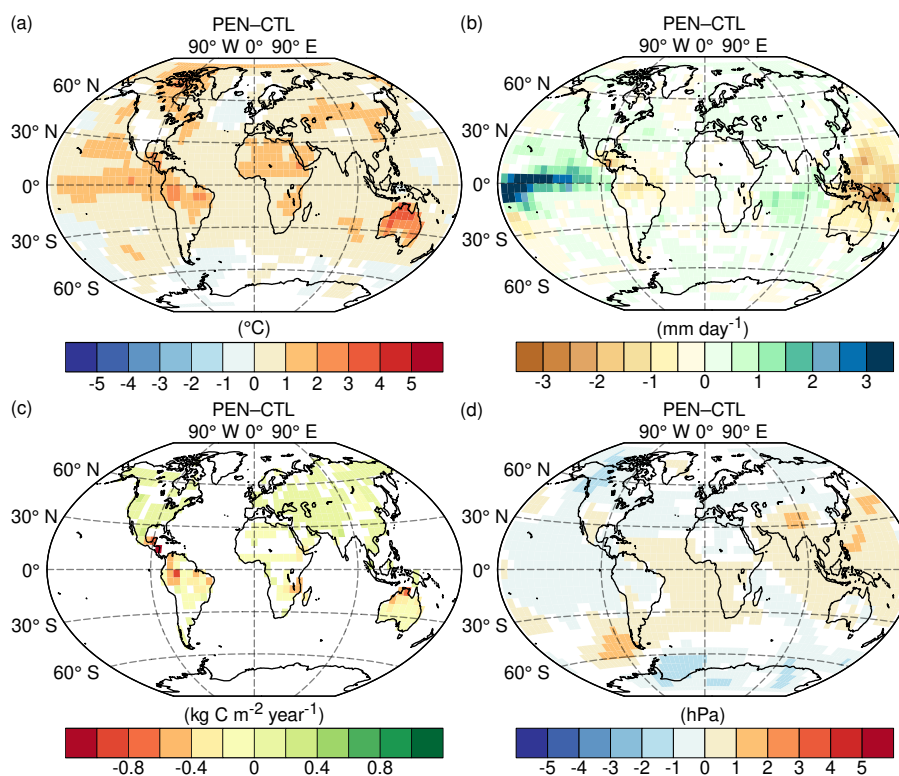
Figure 6. Differences in annual means results for the PEN simulation compared with the CTL simulation (PEN minus CTL) of: (a) near surface temperature, (b) daily precipitation, (c) GPP and (d) mean sea level pressure. In all panels, white depicts gridpoints with statistically non-significant difference ($\alpha = 0.05$).

There are statistically significant differences in the near surface air temperatures for the PEN scenario as compared to the CTL simulation (Fig. 6a). PEN has an average global increase of approximately 0.6 °C. This temperature change is greater on land with an average 1.0 °C increase, than over the oceans, where the change reaches 0.5 °C. In the tropics, variation occurs mainly in the equatorial Pacific region (as expected), but also in Central America, northern South America, Amazonia, the

5   Sahel region in Africa, and northern Australia. Moreover, air over the North Atlantic Ocean is slightly colder, while the Arctic Ocean near Canada and Siberia is warmer. Air over some areas in the southern hemisphere oceans close to Antarctica becomes colder in PEN than in CTL. Seasonally, boreal winter (DJF) shows the greatest warming on land, especially for Australia (Fig. S6a). South America is the warmest during boreal summer (JJA).

Regarding precipitation, PEN leads to an average rise in ocean precipitation of approximately 0.1 mm day^{-1} and a decrease

10   in continental areas of about the same value (Fig. 6b). Precipitation over the tropical Atlantic Ocean is also slightly reduced in the PEN scenario. On land the most conspicuous differences occur near the equator, in Central America and in the Amazon, where precipitation is reduced. Conversely, in the northern hemisphere above midlatitudes, land areas experience higher pre-

cipitation rates. Similar to temperature, boreal winter (DJF) exhibits the largest deviations (Fig. S6b), with above (below) CTL rainfall in equatorial eastern (western) Pacific Ocean.

Higher temperatures and precipitation rates in the temperate zones result in higher productivity rates (Fig. 6c). The opposite happens in regions where temperatures increase while precipitation rates decrease, as in Central America and northern South

5 America and Amazonia. In Africa, in eastern Sahara, there is a relatively small increase in productivity related to increased precipitation. On the contrary, near the Sahel region there is a decay in GPP where precipitation declined with respect to the CTL simulation. The same happens in Australia. Globally, a decrease in productivity of about $0.1 \, \mathrm{kg \, C \, m^{-2} \, year^{-1}}$ occurs in the PEN scenario. PEN results also indicate a decreased productivity in South America (Fig. S7a) during boreal spring (MAM) and summer (JJA).

10 PEN simulation outputs show the Southern Oscillation hemispheric zonal dipole in surface pressure (Fig. 6d). In the Tropics, there is an overall increase in surface pressure over the oceans, which is related to drier air and reduced transport of moisture into continental areas. The opposite is seen in the northern hemisphere midlatitudes, where a slight decrease in surface pressure can be linked to increased precipitation rate. As expected, lower (higher) surface pressure conditions remain year-round in eastern (western) equatorial Pacific Ocean (Fig. S7b). The North Atlantic region has lower surface pressure throughout the year, but

15 most markedly in boreal winter (DJF).

The atmosphere becomes warmer in PEN than it is in the CTL simulation at most pressure levels and latitudes (Fig. S8a). There is a cold bias only near the surface at the austral pole, and also in the northern hemisphere above 500 hPa. The hot spot in the tropics in the upper troposphere is much warmer in the PEN simulation. This result has been previously reported and seems to be related to changes in the radiative forcing of the troposphere layer (Lin et al., 2017). Wind speed increases eastward

20 (or lessens westward) in the model atmosphere (Fig. S8b). Notably, in the midlatitudes in the middle troposphere, the zonal velocity rises eastward, moving the sub-tropical jet streams towards the equator as commonly seen during El Niño conditions. As for the Hadley and Ferrell cells (Fig. S8c), their magnitude increases slightly in both hemispheres, as has been previously stated (Oort and Yienger, 1996).

4.3 Climatological water deficit

25 Our results for both MAP and MCWD are shown in Fig. 7. In terms of MAP, PEN clearly shows rainfall decline in the tropics, whereas it indicates increases in northern temperate and boreal latitudes. Results are similar for MCWD, though most vulnerable areas can be identified as: Amazon rainforest, West Africa, south-eastern Africa and Australia.

The composite map described in Section 3.3 is shown in Fig. 8. According to these results, tropical ecosystems seem to be the most vulnerable to a PEN scenario, whereas temperate and boreal ecosystems could enhance their primary productivity. This

30 is clearly shown in Fig. 9, where most gridpoints in the tropics (30° S–30° N) shift towards much less precipitation conditions with greater water deficits (see the shift to the left). Using a similar approach as Malhi et al. (2009) for Amazonia, but in a global context in the tropics, it seems that a PEN scenario can shift terrestrial ecosystems towards more arid conditions. In the case of boreal and northern temperate (above 30° N) ecosystems, a PEN scenario drives them towards wetter conditions (see the shift to the right).
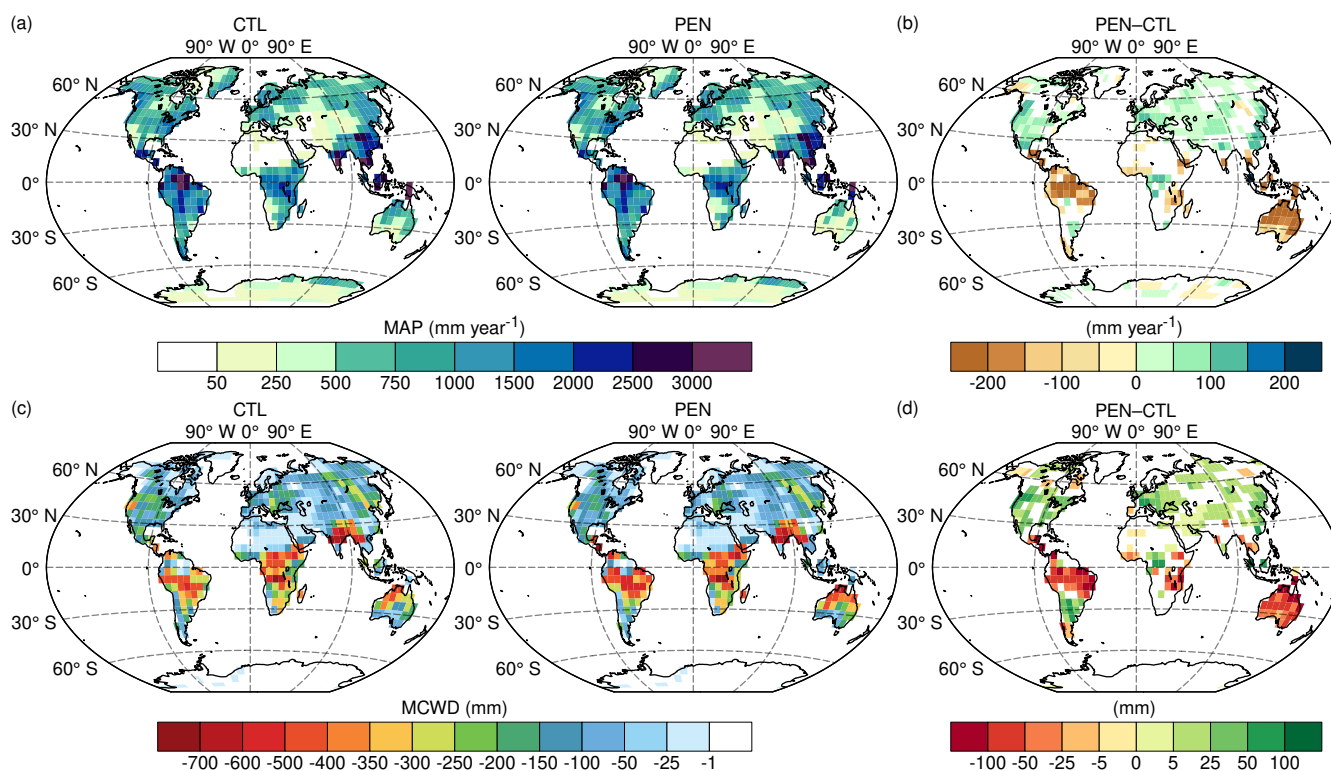
Figure 7. Annual mean results for the PEN simulation compared with the CTL simulation of: (a) MAP in CTL and PEN and (b) their absolute difference, and (b) MCWD in CTL and PEN and (d) their absolute difference. In the difference panels, white depicts gridpoints with statistically non-significant difference ($\alpha = 0.05$).

5 Discussion

Global terrestrial ecosystems can have alternative stable equilibrium sates (Scheffer et al., 2001), and can shift between them when external perturbations and/or internal dynamics force them past critical thresholds (Barnosky et al., 2012; Andersen et al., 2009). Alternative equilibria have already been identified for some biomes in the world. In tropical South America, in

5   the eastern Amazon river basin, where there is currently a rainforest, simulation results suggest the presence of an alternative savannah (Cerrado) state (Oyama and Nobre, 2003). In both the Sahara and Sahel regions in northern Africa, geological records and modelling results suggest that environmental conditions could have supported a "green Sahara" and a "wet Sahel", but climate shifts and atmosphere-vegetation feedback mechanisms could have stabilized their current contrasting states (Brovkin et al., 1998; Foley et al., 2003). Similarly for the wet Tropics in Australia, bi-stability between rainforest and savannah-like

10   sclerophyll land cover has also been studied (Warman and Moles, 2009). Forest, savannah and desert seem to be three possible alternative stable states for terrestrial ecosystems (Hirota et al., 2011; Staver et al., 2011).
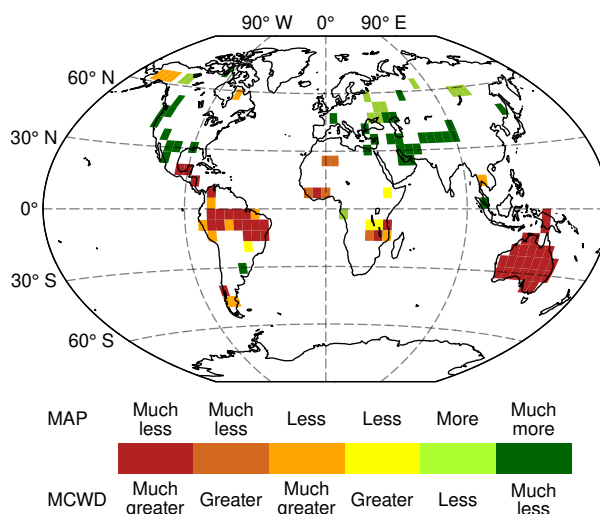
Figure 8. Map of regions where the PEN scenario had the largest differences in terms of MAP and MCWD, with respect to the CTL simulation.

Malhi et al. (2009) studied the possibility of a climate-change-induced state transition in the Amazon rainforest. Estimating water availability and accumulated water stress along a dry season, they identified transition areas between rainforest and savannah alternative states for this large-scale ecosystem. Here we extended this approach to other global ecosystems in order to evaluate whether a PEN scenario could trigger state transitions not only in the Amazon but also in other global ecosystems.

5 The most noticeable effects suggested by the PlaSim model include a potential dieback of the Amazon rainforest, potential expansion of the Sahel area, drying of south-eastern Africa, and further aridification of Australia.

Our results show that PEN can be a driver of forest dieback in the Amazon. El Niño reduces annual precipitation and increases the water deficit across the dry season for this region (Cox et al., 2004; Malhi et al., 2009). This rainfall reduction could perhaps threaten the existence of parts of the rainforest because resilience to dry conditions is limited and a long-lasting

10 drought can increase tree mortality (Phillips et al., 2009). Most forest species operate within a narrow margin of hydraulic safety and therefore are vulnerable to drought-induced embolisms which reduce productivity and increase the risk of forest decline (Choat et al., 2012). Additionally, El Niño-induced fires (not simulated by PlaSim) could further exacerbate forest degradation or transition from evergreen to seasonal tropical forests (Barlow and Peres, 2004; Brando et al., 2014). Consequences of this are manifold, but one important aspect to consider is the global effects the Amazon rainforest has as a carbon sink (Cox et al.,

15 2004; Pan et al., 2011). A PEN-induced dieback in the Amazon could *tip* the rainforest from a sink of carbon to a possible source (Davidson et al., 2012). This could in turn amplify the magnitude of extreme hydrological and weather events that occur during El Niño, such as droughts, in a positive-feedback-like manner (Zemp et al., 2017; Salazar et al., 2018), as well as disrupt mechanisms of river flow regulation (Salazar et al., 2018; Mercado-Bettin et al., 2019) and continental precipitation distribution (Molina et al., 2019). Near-synchronous effects of this sort between different *tipping elements* could give rise

20 to a "tipping cascade" that could contribute to a planetary-scale state shift (Lenton and Williams, 2013). Despite potential
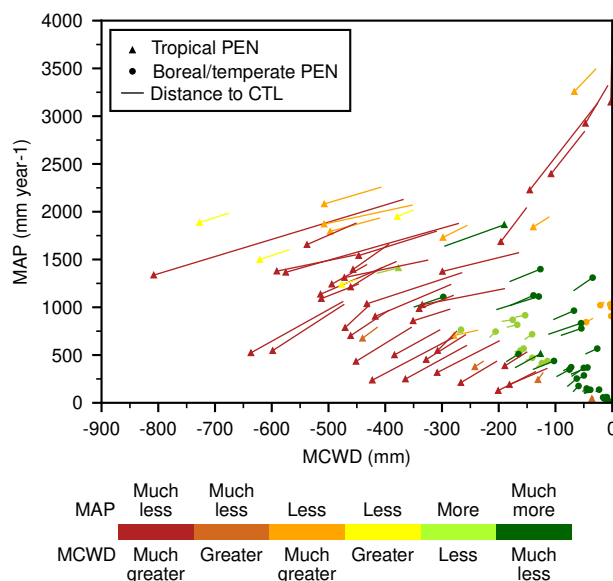
Figure 9. Changes in MAP and MCWD in the PEN scenario compared to the CTL scenario. Distinct markers are used to differentiate tropical (30° S–30° N; solid triangles) from boreal and northern temperate (above 30° N; solid circles) gridpoints results for PEN scenario, and a straight line shows the distance to the value it had for the CTL scenario. Each line corresponds to a cell with significant change shown in Figure 8.

forest collapse in most of the Amazon, our results also agree with Betts et al. (2008) that some areas in western Amazonia (adjacent to the Andes) are less vulnerable and could act as a refuge for biodiversity. Consequences of a PEN scenario in the Amazon rainforest would have global impact, since it is the largest remaining intact forest in the world, which provide globally significant environmental benefits (Watson et al., 2018).

5   The influence of ENSO on rainfall patterns in south-eastern Africa was identified long ago (Nicholson and Kim, 1997). This happens directly via atmospheric teleconnections (Ratnam et al., 2014) and also through warming of the Indian and Atlantic oceans (Giannini et al., 2008). El Niño in this region is linked to below average rainfall and droughts (Rouault and Richard, 2005). This is present in our results south of the Great Horn of Africa, where the PEN scenario creates a greater water deficit and much less precipitation. Our results agree with Gizaw and Gan (2017), who discussed the impact on Africa of increased

10   frequency of El Niño episodes using climate projections and state-of-the-art general circulation models. They also found south-eastern Africa to be particularly vulnerable. Earlier modelling studies found that such savannah ecosystems in Africa are closely related to climate variability, which keeps the system in between desert-like and forest-like equilibrium states (Zeng and Neelin, 2000). More recent work also associates the savannah equilibrium state to rainfall variability (Staver et al., 2011). Hence, tipping the ENSO permanently could trigger land cover transitions from forest to savannah and/or savannah to desert-

15   like biomes. This is problematic not only in terms of ecosystem degradation, but also in terms of putting at risk food security and hydro-power generation (Lyon, 2014). In the case of West Africa, the impacts of ENSO have been contested because of

the many other climatic drivers that come together in this area (Nicholson, 2013). However, ENSO events have been linked to climatic variability in both the Sahel and Guinea coastal regions (Sheen et al., 2017; Joly and Voldoire, 2009; Tippett and Giannini, 2006). These two regions are connected via the West African monsoon in boreal summer, which brings moisture inland from the Atlantic Ocean (Nicholson et al., 2017). During El Niño conditions, a coherent drying pattern for the Sahel has

5   been identified (Pomposi et al., 2016). PlaSim simulation results also support the role of the warm ENSO phase in modulating rainfall in West Africa, and show it leads to a drier state in southern Sahel and Guinea Coast regions. This southward expansion of the Sahel dry conditions into Guinea Coast, agrees with the notion of potential enlargement of the world's deserts due to climate change (Zeng and Yoon, 2009). A PEN scenario could push arid and semi-arid ecosystems into vegetation-atmosphere positive feedbacks of desertification.

10 El Niño events have had different effects on rainfall in Australia, depending on how far east the Walker circulation moves (Wang and Hendon, 2007). In this case, we show that a PEN based on the strong El Niño of 2015–2016 is able to alter climate with potentially severe ecological consequences. Likewise, in spite of observed weakening of teleconnections between Australia rainfall and ENSO (Ashcroft et al., 2016), our results indicate that a PEN scenario could cause significant widespread aridification of Australia. Coupling this process with land cover changes, could give rise to synergistic effects that could

15 potentially *tip* Australia's climate towards a much drought-prone state (McAlpine et al., 2009). Furthermore, extreme weather events (such as droughts) and changes in local hydrology, have been identified as key drivers of terrestrial and marine Australian ecosystems towards tipping points (Laurance et al., 2011). Hence, following our results, a PEN could originate a "tipping cascade" in this continent.

Contrasting results were found for temperate and boreal ecosystems, where the PEN scenario leads to increased rainfall

20 accompanied with a reduction in cumulative water deficit and increased productivity. This is consistent with earlier findings for El Niño years in forests, because warmer temperatures allow milder winter seasons leading to greater productivity (Malhi et al., 1999). Thus the response of tropical, temperate and boreal ecosystems to PEN seems to be asymmetric: while tropical ecosystems are degraded (GPP is generally reduced), temperate and boreal ecosystems are enhanced (GPP increases). This, combined with land cover changes (human or PEN induced) could turn tropical biomes into global net sources of carbon that,

25 according to current estimates (Pan et al., 2011), could not be counter-balanced by extra-tropical forests.

6   Conclusions

This study has provided additional evidence that PlaSim can realistically represent the current state of the Earth's climate system. Despite its coarse resolution and simplified parameterizations, the model is able to display the large-scale patterns of atmospheric dynamics seen in observational data sets. In describing some of its limitations, we found that it displays common

30 biases seen in other state-of-the-art climate models. Therefore, PlaSim provides an adequate framework to study the dynamics of the earth system (as a whole), including complex climate feedbacks, using long simulations.

Our key finding is that a permanent tipping of the ENSO into a very strong warm phase (El Niño) can trigger state transitions in global terrestrial ecosystems, with asymmetric effects between the tropics and extra-tropical regions. We identified some

regions that seem to be more susceptible to shifting into more arid biomes: the Amazon rainforest, tropical western and south-eastern Africa and Australia. These results also suggest the possibility that a permanent El Niño can trigger tipping cascades. It is important to mention that despite there being other sources of variability for these ecosystems (for instance the Atlantic Ocean temperatures variation), here we focused only on the consequences that an observed-very-strong-El Niño-based SST

5   climatology could have on continental areas, without linking any simulated anomalies to a specific region in space. This means that despite the Pacific Ocean shows the largest anomalies (as in El Niño) we cannot attribute all of our results to changes only in this region. Even though a modelling study of this sort is not enough to prove that such state shifts will occur in a climate change scenario, it does show a consistent picture, and should raise concern about the conservation of global ecosystems and related water resources management practices in a world with more frequent and/or intense El Niño events (Latif et al., 2015;

10   Cai et al., 2014).

Data availability. All observational data sets and reanalyses used in this study are publicly available online. Model results are readily available upon request.

Author contributions. All authors participated in the design of the experiments and the discussion of the results.

Competing interests. The authors declare that they have no conflict of interest.

15   *Acknowledgements.* MD-V was funded by Universidad de Antioquia through the "Estudiante Instructor" program. JFS and AMR were partially supported by "Programa de investigación en la gestión de riesgo asociado con cambio climático y ambiental en cuencas hidrográficas" (UT-GRA), Convocatoria 543–2011 Colciencias. We thank Daniel Ruiz Carrascal and Luis F. Salazar for insightful comments on an early version of this manuscript.

References

Adler, R. F., Huffman, G. J., Chang, A., Ferraro, R., Xie, P.-P., Janowiak, J., Rudolf, B., Schneider, U., Curtis, S., Bolvin, D., et al.: The Version-2 Global Precipitation Climatology Project (GPCP) Monthly Precipitation Analysis (1979-Present), Journal of Hydrometeorology, 4, 1147–1167, https://doi.org/10.1175/1525-7541(2003)004<1147:TVGPCP>2.0.CO;2, 2003.

5 Alencar, A., Nepstad, D., and Diaz, M. C. V.: Forest understory fire in the Brazilian Amazon in ENSO and non-ENSO years: area burned and committed carbon emissions, Earth Interactions, 10, 1–17, https://doi.org/10.1175/EI150.1, 2006.

Allan, R. and Ansell, T.: A New Globally Complete Monthly Historical Gridded Mean Sea Level Pressure Dataset (HadSLP2): 1850-2004, Journal of Climate, 19, 5816–5842, https://doi.org/10.1175/JCLI3937.1, 2006.

Andersen, T., Carstensen, J., Hernandez-Garcia, E., and Duarte, C. M.: Ecological Thresholds And Regime Shifts: Approaches To Identifi-

10 cation, Trends in Ecology & Evolution, 24, 49–57, https://doi.org/10.1016/j.tree.2008.07.014, 2009.

Aragao, L. E. O., Malhi, Y., Roman-Cuesta, R. M., Saatchi, S., Anderson, L. O., and Shimabukuro, Y. E.: Spatial Patterns And Fire Response Of Recent Amazonian Droughts, Geophysical Research Letters, 34, https://doi.org/10.1029/2006GL028946, 2007.

Arakawa, A.: The cumulus parameterization problem: past, present, and future, Journal of Climate, 17, 2493–2525, 2004.

Ardö, J.: Comparison between remote sensing and a dynamic vegetation model for estimating terrestrial primary production of Africa,

15 Carbon balance and management, 10, 8, 2015.

Ashcroft, L., Gergis, J., and Karoly, D. J.: Long-term Stationarity Of El Niño-Southern Oscillation Teleconnections In Southeastern Australia, Climate dynamics, 46, 2991–3006, https://doi.org/10.1007/s00382-015-2746-3, 2016.

Ashok, K., Behera, S. K., Rao, S. A., Weng, H., and Yamagata, T.: El Niño Modoki and its possible teleconnection, Journal of Geophysical Research: Oceans, 112, 1–27, 2007.

20 Barlow, J. and Peres, C. A.: Ecological Responses To El Niño-Induced Surface Fires In Central Brazilian Amazonia: Management Implications For Flammable Tropical Forests, Philosophical Transactions of the Royal Society of London B: Biological Sciences, 359, 367–380, https://doi.org/10.1098/rstb.2003.1423, 2004.

Barnosky, A. D., Hadly, E. A., Bascompte, J., Berlow, E. L., Brown, J. H., Fortelius, M., Getz, W. M., Harte, J., Hastings, A., Marquet, P. A., et al.: Approaching A State Shift In Earth's Biosphere, Nature, 486, 52–58, https://doi.org/10.1038/nature11018, 2012.

25 Bathiany, S., Claussen, M., and Fraedrich, K.: Implications Of Climate Variability For The Detection Of Multiple Equilibria And For Rapid Transitions In The Atmosphere-Vegetation System, Climate Dynamics, 38, 1775–1790, https://doi.org/10.1007/s00382-011-1037-x, 2012.

Betts, R. A., Malhi, Y., and Roberts, J. T.: The Future Of The Amazon: New Perspectives From Climate, Ecosystem And Social Sciences, Philosophical Transactions of the Royal Society B: Biological Sciences, 363, 1729–1735, https://doi.org/10.1098/rstb.2008.0011, 2008.

Boschi, R., Lucarini, V., and Pascale, S.: Bistability Of The Climate Around The Habitable Zone: A Thermodynamic Investigation, Icarus,

30 226, 1724–1742, https://doi.org/10.1016/j.icarus.2013.03.017, 2013.

Brando, P. M., Balch, J. K., Nepstad, D. C., Morton, D. C., Putz, F. E., Coe, M. T., Silvério, D., Macedo, M. N., Davidson, E. A., Nóbrega, C. C., et al.: Abrupt Increases In Amazonian Tree Mortality Due To Drought-Fire Interactions, Proceedings of the National Academy of Sciences, 111, 6347–6352, https://doi.org/10.1073/pnas.1305499111, 2014.

Brovkin, V., Claussen, M., Petoukhov, V., and Ganopolski, A.: On The Stability Of The Atmosphere-Vegetation System In The Sahara/Sahel

35 Region, Journal of Geophysical Research: Atmospheres, 103, 31 613–31 624, https://doi.org/10.1029/1998JD200006, 1998.

Cai, W., Borlace, S., Lengaigne, M., Van Rensch, P., Collins, M., Vecchi, G., Timmermann, A., Santoso, A., McPhaden, M. J., Wu, L., et al.: Increasing Frequency Of Extreme El Niño Events Due To Greenhouse Warming, Nature climate change, 4, 111–116, https://doi.org/10.1038/nclimate2100, 2014.

Cai, W., Santoso, A., Wang, G., Yeh, S.-W., An, S.-I., Cobb, K. M., Collins, M., Guilyardi, E., Jin, F.-F., Kug, J.-S., et al.: ENSO And
5   Greenhouse Warming, Nature Climate Change, 5, 849–859, https://doi.org/10.1038/nclimate2743, 2015.

Choat, B., Jansen, S., Brodribb, T. J., Cochard, H., Delzon, S., Bhaskar, R., Bucci, S. J., Feild, T. S., Gleason, S. M., Hacke, U. G., et al.: Global Convergence In The Vulnerability Of Forests To Drought, Nature, 491, 752–755, https://doi.org/10.1038/nature11688, 2012.

Claussen, M., Mysak, L., Weaver, A., Crucifix, M., Fichefet, T., Loutre, M.-F., Weber, S., Alcamo, J., Alexeev, V., Berger, A., et al.: Earth System Models Of Intermediate Complexity: Closing The Gap In The Spectrum Of Climate System Models, Climate dynamics, 18,
10   579–586, https://doi.org/10.1007/s00382-001-0200-1, 2002.

Costa, M. H. and Pires, G. F.: Effects Of Amazon And Central Brazil Deforestation Scenarios On The Duration Of The Dry Season In The Arc Of Deforestation, International Journal of Climatology, 30, 1970–1979, https://doi.org/10.1002/joc.2048, 2010.

Cox, P. M., Betts, R., Collins, M., Harris, P. P., Huntingford, C., and Jones, C.: Amazonian Forest Dieback Under Climate-Carbon Cycle Projections For The 21st Century, Theoretical and applied climatology, 78, 137–156, https://doi.org/10.1007/s00704-004-0049-4, 2004.

15 Davidson, E. A., de Araújo, A. C., Artaxo, P., Balch, J. K., Brown, I. F., Bustamante, M. M., Coe, M. T., DeFries, R. S., Keller, M., Longo, M., et al.: The Amazon Basin In Transition, Nature, 481, 321–328, https://doi.org/10.1038/nature10717, 2012.

Dee, D. P., Uppala, S. M., Simmons, A. J., Berrisford, P., Poli, P., Kobayashi, S., Andrae, U., Balmaseda, M. A., Balsamo, G., Bauer, P., Bechtold, P., Beljaars, A. C. M., van de Berg, L., Bidlot, J., Bormann, N., Delsol, C., Dragani, R., Fuentes, M., Geer, A. J., Haimberger, L., Healy, S. B., Hersbach, H., Hólm, E. V., Isaksen, L., Kållberg, P., Köhler, M., Matricardi, M., McNally, A. P., Monge-Sanz, B. M.,
20   Morcrette, J.-J., Park, B.-K., Peubey, C., de Rosnay, P., Tavolato, C., Thépaut, J.-N., and Vitart, F.: The ERA-Interim Reanalysis: Configuration And Performance Of The Data Assimilation System, Quarterly Journal of the Royal Meteorological Society, 137, 553–597, https://doi.org/10.1002/qj.828, 2011.

Dekker, S., De Boer, H., Brovkin, V., Fraedrich, K., Wassen, M., and Rietkerk, M.: Biogeophysical Feedbacks Trigger Shifts In The Modelled Vegetation-Atmosphere System At Multiple Scales, Biogeosciences, 7, 1237–1245, https://doi.org/10.5194/bg-7-1237-2010, 2010.

25 Diaz, H. F. and Markgraf, V.: El Niño and the Southern Oscillation: Multiscale variability and global and regional impacts, Cambridge University Press, 2000.

Flato, G., Marotzke, J., Abiodun, B., Braconnot, P., Chou, S. C., Collins, W. J., Cox, P., Driouech, F., Emori, S., Eyring, V., et al.: Evaluation Of Climate Models, in: Climate Change 2013: the Physical Science Basis. Contribution of Working Group I to the Fifth Assessment Report of the Intergovernmental Panel on Climate Change, pp. 741–866, Cambridge University Press,
30   https://doi.org/10.1017/CBO9781107415324.020, 2013.

Foley, J. A., Botta, A., Coe, M. T., and Costa, M. H.: El Niño-Southern Oscillation and the climate, ecosystems and rivers of Amazonia, Global biogeochemical cycles, 16, 1132, https://doi.org/10.1029/2002GB001872, 2002.

Foley, J. A., Coe, M. T., Scheffer, M., and Wang, G.: Regime Shifts In The Sahara And Sahel: Interactions Between Ecological And Climatic Systems In Northern Africa, Ecosystems, 6, 524–532, https://doi.org/10.1007/s10021-002-0227-0, 2003.

35 Fraedrich, K.: A Suite Of User-Friendly Global Climate Models: Hysteresis Experiments, The European Physical Journal Plus, 127, 53, https://doi.org/10.1140/epjp/i2012-12053-7, 2012.

Fraedrich, K., Jansen, H., Kirk, E., Luksch, U., and Lunkeit, F.: The Planet Simulator: Towards A User Friendly Model, Meteorologische Zeitschrift, 14, 299–304, https://doi.org/10.1127/0941-2948/2005/0043, 2005a.

Fraedrich, K., Jansen, H., Kirk, E., and Lunkeit, F.: The Planet Simulator: Green Planet And Desert World, Meteorologische Zeitschrift, 14, 305–314, https://doi.org/10.1127/0941-2948/2005/0044, 2005b.

Fraedrich, K., Kirk, E., Luksch, U., and Lunkeit, F.: The Portable University Model Of The Atmosphere (PUMA): Storm Track Dynamics And Low-Frequency Variability, Meteorologische Zeitschrift, 14, 735–745, https://doi.org/10.1127/0941-2948/2005/0074, 2005c.

5 Garreaud, R. D., Molina, A., and Farias, M.: Andean Uplift, Ocean Cooling And Atacama Hyperaridity: A Climate Modeling Perspective, Earth and Planetary Science Letters, 292, 39–50, https://doi.org/10.1016/j.epsl.2010.01.017, 2010.

Giannini, A., Biasutti, M., Held, I. M., and Sobel, A. H.: A Global Perspective On African Climate, Climatic Change, 90, 359–383, https://doi.org/10.1007/s10584-008-9396-y, 2008.

Gizaw, M. S. and Gan, T. Y.: Impact Of Climate Change And El Niño Episodes On Droughts In Sub-Saharan Africa, Climate Dynamics, 49,
10 665–682, https://doi.org/10.1007/s00382-016-3366-2, 2017.

Guilyardi, E.: El Niño-mean state-seasonal cycle interactions in a multi-model ensemble, Climate Dynamics, 26, 329–348, 2006.

Henrot, A.-J., François, L., Brewer, S., and Munhoven, G.: Impacts Of Land Surface Properties And Atmospheric CO_2 On The Last Glacial Maximum Climate: A Factor Separation Analysis, Climate of the Past, 5, 183–202, https://doi.org/10.5194/cp-5-183-2009, 2009.

Hirota, M., Holmgren, M., Van Nes, E. H., and Scheffer, M.: Global resilience of tropical forest and savanna to critical transitions, Science,
15 334, 232–235, https://doi.org/10.1126/science.1210657, 2011.

Holmgren, M., Scheffer, M., Ezcurra, E., Gutiérrez, J. R., and Mohren, G. M.: El Niño Effects On The Dynamics Of Terrestrial Ecosystems, Trends in Ecology & Evolution, 16, 89–94, https://doi.org/10.1016/S0169-5347(00)02052-8, 2001.

Holmgren, M., Stapp, P., Dickman, C. R., Gracia, C., Graham, S., Gutiérrez, J. R., Hice, C., Jaksic, F., Kelt, D. A., Letnic, M., et al.: A synthesis of ENSO effects on drylands in Australia, North America and South America, Advances in Geosciences, 6, 69–72,
20 https://doi.org/10.5194/adgeo-6-69-2006, 2006.

Hoskins, B. and Simmons, A.: A multi-layer spectral model and the semi-implicit method, Quarterly Journal of the Royal Meteorological Society, 101, 637–655, https://doi.org/10.1002/qj.49710142918, 1975.

Hurrell, J. W., Hack, J. J., Shea, D., Caron, J. M., and Rosinski, J.: A New Sea Surface Temperature And Sea Ice Boundary Dataset For The Community Atmosphere Model, Journal of Climate, 21, 5145–5153, https://doi.org/10.1175/2008JCLI2292.1, 2008.

25 Indeje, M., Semazzi, F. H., and Ogallo, L. J.: ENSO signals in East African rainfall seasons, International journal of Climatology, 20, 19–46, https://doi.org/10.1002/(SICI)1097-0088(200001)20:1<19::AID-JOC449>3.0.CO;2-0, 2000.

Jiménez-Muñoz, J. C., Mattar, C., Barichivich, J., Santamaría-Artigas, A., Takahashi, K., Malhi, Y., Sobrino, J. A., and van der Schrier, G.: Record-Breaking Warming And Extreme Drought In The Amazon Rainforest During The Course Of El Niño 2015-2016, Scientific Reports, 6, 33 130, https://doi.org/10.1038/srep33130, 2016.

30 Joly, M. and Voldoire, A.: Influence Of ENSO On The West African Monsoon: Temporal Aspects And Atmospheric Processes, Journal of Climate, 22, 3193–3210, https://doi.org/10.1175/2008JCLI2450.1, 2009.

Kleidon, A.: The Climate Sensitivity To Human Appropriation Of Vegetation Productivity And Its Thermodynamic Characterization, Global and Planetary Change, 54, 109–127, https://doi.org/10.1016/j.gloplacha.2006.01.016, 2006.

Kleidon, A.: Non-Equilibrium Thermodynamics, Maximum Entropy Production And Earth-System Evolution, Philosophical Transactions of
35 the Royal Society of London A: Mathematical, Physical and Engineering Sciences, 368, 181–196, https://doi.org/10.1098/rsta.2009.0188, 2010.

Kunz, T., Fraedrich, K., and Lunkeit, F.: Response Of Idealized Baroclinic Wave Life Cycles To Stratospheric Flow Conditions, Journal of the Atmospheric Sciences, 66, 2288–2302, https://doi.org/10.1175/2009JAS2827.1, 2009.

Latif, M., Semenov, V. A., and Park, W.: Super El Niños In Response To Global Warming In A Climate Model, Climatic Change, 132, 489–500, https://doi.org/10.1007/s10584-015-1439-6, 2015.

Laurance, W. F., Dell, B., Turton, S. M., Lawes, M. J., Hutley, L. B., McCallum, H., Dale, P., Bird, M., Hardy, G., Prideaux, G., et al.: The 10 Australian Ecosystems Most Vulnerable To Tipping Points, Biological Conservation, 144, 1472–1480, https://doi.org/10.1016/j.biocon.2011.01.016, 2011.

Leitold, V., Morton, D. C., Longo, M., dos Santos, M. N., Keller, M., and Scaranello, M.: El Niño Drought Increased Canopy Turnover In Amazon Forests, New Phytologist, https://doi.org/10.1111/nph.15110, 2018.

Lenton, T. M.: Early Warning Of Climate Tipping Points, Nature Climate Change, 1, 201–209, https://doi.org/10.1038/nclimate1143, 2011.

Lenton, T. M. and Ciscar, J.-C.: Integrating Tipping Points Into Climate Impact Assessments, Climatic Change, 117, 585–597, https://doi.org/10.1007/s10584-012-0572-8, 2013.

Lenton, T. M. and Williams, H. T.: On The Origin Of Planetary-Scale Tipping Points, Trends in ecology & evolution, 28, 380–382, https://doi.org/10.1016/j.tree.2013.06.001, 2013.

Lenton, T. M., Held, H., Kriegler, E., Hall, J. W., Lucht, W., Rahmstorf, S., and Schellnhuber, H. J.: Tipping Elements In The Earth's Climate System, Proceedings of the National Academy of Sciences, 105, 1786–1793, https://doi.org/10.1073/pnas.0705414105, 2008.

Lin, J.-L.: The double-ITCZ problem in IPCC AR4 coupled GCMs: Ocean-atmosphere feedback analysis, Journal of Climate, 20, 4497–4525, 2007.

Lin, P., Paynter, D., Ming, Y., and Ramaswamy, V.: Changes of the tropical tropopause layer under global warming, Journal of Climate, 30, 1245–1258, 2017.

Linsenmeier, M., Pascale, S., and Lucarini, V.: Climate Of Earth-Like Planets With High Obliquity And Eccentric Orbits: Implications For Habitability Conditions, Planetary and Space Science, 105, 43–59, https://doi.org/10.1016/j.pss.2014.11.003, 2015.

Lucarini, V., Fraedrich, K., and Lunkeit, F.: Thermodynamic Analysis Of Snowball Earth Hysteresis Experiment: Efficiency, Entropy Production And Irreversibility, Quarterly Journal of the Royal Meteorological Society, 136, 2–11, https://doi.org/10.1002/qj.543, 2010.

Lucarini, V., Pascale, S., Boschi, R., Kirk, E., and Iro, N.: Habitability And Multistability In Earth-Like Planets, Astronomische Nachrichten, 334, 576–588, https://doi.org/10.1002/asna.201311903, 2013.

Lucarini, V., Ragone, F., and Lunkeit, F.: Predicting Climate Change Using Response Theory: Global Averages And Spatial Patterns, Journal of Statistical Physics, 166, 1036–1064, https://doi.org/10.1007/s10955-016-1506-z, 2017.

Lunkeit, F., Borth, H., Böttinger, M., Fraedrich, K., Jansen, H., Kirk, E., Kleidon, A., Luksch, U., Paiewonsky, P., Schubert, S., Sielmann, S., and Wan, H.: Planet Simulator Reference Manual Version 16, Meteorologisches Institut, Universität Hamburg, 2011.

Lyon, B.: Seasonal Drought In The Greater Horn Of Africa And Its Recent Increase During The March-May Long Rains, Journal of Climate, 27, 7953–7975, https://doi.org/10.1175/JCLI-D-13-00459.1, 2014.

Malhi, Y., Aragão, L. E., Galbraith, D., Huntingford, C., Fisher, R., Zelazowski, P., Sitch, S., McSweeney, C., and Meir, P.: Exploring The Likelihood And Mechanism Of A Climate-Change-Induced Dieback Of The Amazon Rainforest, Proceedings of the National Academy of Sciences, 106, 20 610–20 615, https://doi.org/10.1073/pnas.0804619106, 2009.

Malhi, Y. a., Baldocchi, D., and Jarvis, P.: The Carbon Balance Of Tropical, Temperate And Boreal Forests, Plant, Cell & Environment, 22, 715–740, https://doi.org/10.1046/j.1365-3040.1999.00453.x, 1999.

McAlpine, C., Syktus, J., Ryan, J., Deo, R., McKeon, G., McGowan, H., and Phinn, S.: A Continent Under Stress: Interactions, Feedbacks And Risks Associated With Impact Of Modified Land Cover On Australia's Climate, Global Change Biology, 15, 2206–2223, https://doi.org/10.1111/j.1365-2486.2009.01939.x, 2009.

McPhaden, M. J., Zebiak, S. E., and Glantz, M. H.: ENSO As An Integrating Concept In Earth Science, Science, 314, 1740–1745, https://doi.org/10.1126/science.1132588, 2006.

Mercado-Bettin, D., Salazar, J., and Villegas, J.: Long-term water balance partitioning explained by physical and ecological characteristics in world river basins, Ecohydrology, p. e2072, https://doi.org/10.1002/eco.2072, 2019.

5 Molina, R. D., Salazar, J. F., Martínez, J. A., Villegas, J. C., and Arias, P. A.: Forest-induced exponential growth of precipitation along climatological wind streamlines over the Amazon, Journal of Geophysical Research: Atmospheres, 124, https://doi.org/10.1029/2018JD029534, 2019.

Morice, C. P., Kennedy, J. J., Rayner, N. A., and Jones, P. D.: Quantifying Uncertainties In Global And Regional Temperature Change Using An Ensemble Of Observational Estimates: The HadCRUT4 Data Set, Journal of Geophysical Research: Atmospheres, 117, 1–22, 10 https://doi.org/10.1029/2011jd017187, 2012.

Nicholson, S. E.: The West African Sahel: A Review Of Recent Studies On The Rainfall Regime And Its Interannual Variability, ISRN Meteorology, 2013, 1–32, https://doi.org/10.1155/2013/453521, 2013.

Nicholson, S. E. and Kim, J.: The Relationship Of The El Niño-Southern Oscillation To African Rainfall, International Journal of Climatology, 17, 117–135, https://doi.org/10.1002/(SICI)1097-0088(199702)17:2<117::AID-JOC84>3.0.CO;2-O, 1997.

15 Nicholson, S. E., Funk, C., and Fink, A. H.: Rainfall Over The African Continent From The 19th Through The 21st Century, Global and Planetary Change, 165, 114–127, https://doi.org/10.1016/j.gloplacha.2017.12.014, 2017.

Oort, A. H. and Yienger, J. J.: Observed Interannual Variability In The Hadley Circulation And Its Connection To ENSO, Journal of Climate, 9, 2751–2767, https://doi.org/10.1175/1520-0442(1996)009<2751:OIVITH>2.0.CO;2, 1996.

Orszag, S. A.: Transform Method For The Calculation Of Vector-Coupled Sums: Application To The Spectral Form Of The Vorticity Equa-
20 tion, Journal of the Atmospheric Sciences, 27, 890–895, https://doi.org/10.1175/1520-0469(1970)027<0890:TMFTCO>2.0.CO;2, 1970.

Oyama, M. D. and Nobre, C. A.: A New Climate-Vegetation Equilibrium State for Tropical South America, Geophysical Research Letters, 30, 2199, https://doi.org/10.1029/2003gl018600, 2003.

Pan, Y., Birdsey, R. A., Fang, J., Houghton, R., Kauppi, P. E., Kurz, W. A., Phillips, O. L., Shvidenko, A., Lewis, S. L., Canadell, J. G., et al.: A Large And Persistent Carbon Sink In The World's Forests, Science, p. 1201609, https://doi.org/10.1126/science.1201609, 2011.

25 Phillips, O. L., Aragão, L. E., Lewis, S. L., Fisher, J. B., Lloyd, J., López-González, G., Malhi, Y., Monteagudo, A., Peacock, J., Quesada, C. A., et al.: Drought Sensitivity Of The Amazon Rainforest, Science, 323, 1344–1347, https://doi.org/10.1126/science.1164033, 2009.

Pithan, F., Shepherd, T. G., Zappa, G., and Sandu, I.: Climate Model Biases In Jet Streams, Blocking And Storm Tracks Resulting From Missing Orographic Drag, Geophysical Research Letters, 43, 7231–7240, https://doi.org/10.1002/2016gl069551, 2016.

Pomposi, C., Giannini, A., Kushnir, Y., and Lee, D. E.: Understanding Pacific Ocean Influence On Interannual Precipitation Variability In
30 The Sahel, Geophysical Research Letters, 43, 9234–9242, https://doi.org/10.1002/2016GL069980, 2016.

Prein, A. F. and Gobiet, A.: Impacts Of Uncertainties In European Gridded Precipitation Observations On Regional Climate Analysis, International Journal of Climatology, 37, 305–327, https://doi.org/10.1002/joc.4706, 2017.

Ratnam, J., Behera, S., Masumoto, Y., and Yamagata, T.: Remote Effects Of El Niño And Modoki Events On The Austral Summer Precipitation Of Southern Africa, Journal of Climate, 27, 3802–3815, https://doi.org/10.1175/JCLI-D-13-00431.1, 2014.

35 Rouault, M. and Richard, Y.: Intensity And Spatial Extent Of Droughts In Southern Africa, Geophysical Research Letters, 32, L15 702, https://doi.org/10.1029/2005GL022436, 2005.

Salazar, J. F., Villegas, J. C., Rendón, A. M., Rodríguez, E., Hoyos, I., Mercado-Bettín, D., and Poveda, G.: Scaling properties reveal regulation of river flows in the Amazon through a forest reservoir, Hydrology and Earth System Sciences, 22, 1735–1748, https://doi.org/10.5194/hess-22-1735-2018, 2018.

Santer, B. D., Solomon, S., Pallotta, G., Mears, C., Po-Chedley, S., Fu, Q., Wentz, F., Zou, C.-Z., Painter, J., Cvijanovic, I., et al.: Comparing
5   tropospheric warming in climate models and satellite data, Journal of Climate, 30, 373–392, 2017.

Sausen, R., Schubert, S., and Dümenil, L.: A model of river runoff for use in coupled atmosphere-ocean models, Journal of Hydrology, 155, 337–352, https://doi.org/10.1016/0022-1694(94)90177-5, 1994.

Scheffer, M., Carpenter, S., Foley, J. A., Folke, C., and Walker, B.: Catastrophic Shifts In Ecosystems, Nature, 413, 591–596, https://doi.org/10.1038/35098000, 2001.

10 Scheffer, M., Bascompte, J., Brock, W. A., Brovkin, V., Carpenter, S. R., Dakos, V., Held, H., Van Nes, E. H., Rietkerk, M., and Sugihara, G.: Early-Warning Signals For Critical Transitions, Nature, 461, 53–59, https://doi.org/10.1038/nature08227, 2009.

Schmittner, A., Silva, T. A., Fraedrich, K., Kirk, E., and Lunkeit, F.: Effects Of Mountains And Ice Sheets On Global Ocean Circulation, Journal of Climate, 24, 2814–2829, https://doi.org/10.1175/2010JCLI3982.1, 2011.

Seager, R. and Henderson, N.: Diagnostic computation of moisture budgets in the ERA-Interim reanalysis with reference to analysis of
15   CMIP-archived atmospheric model data, Journal of Climate, 26, 7876–7901, https://doi.org/10.1175/JCLI-D-13-00018.1, 2013.

Semtner Jr, A. J.: A model for the thermodynamic growth of sea ice in numerical investigations of climate, Journal of Physical Oceanography, 6, 379–389, https://doi.org/10.1175/1520-0485(1976)006<0379:AMFTTG>2.0.CO;2, 1976.

Sheen, K., Smith, D., Dunstone, N., Eade, R., Rowell, D., and Vellinga, M.: Skilful Prediction Of Sahel Summer Rainfall On Inter-Annual And Multi-Year Timescales, Nature Communications, 8, 14 966, https://doi.org/10.1038/ncomms14966, 2017.

20 Spiegl, T., Paeth, H., and Frimmel, H.: Evaluating Key Parameters For The Initiation Of A Neoproterozoic Snowball Earth With A Single Earth System Model Of Intermediate Complexity, Earth and Planetary Science Letters, 415, 100–110, https://doi.org/10.1016/j.epsl.2015.01.035, 2015.

Staver, A. C., Archibald, S., and Levin, S. A.: The Global Extent And Determinants Of Savanna And Forest As Alternative Biome States, Science, 334, 230–232, https://doi.org/10.1126/science.1210465, 2011.

25 Stevens, B., Giorgetta, M., Esch, M., Mauritsen, T., Crueger, T., Rast, S., Salzmann, M., Schmidt, H., Bader, J., Block, K., Brokopf, R., Fast, I., Kinne, S., Kornblueh, L., Lohmann, U., Pincus, R., Reichler, T., and Roeckner, E.: Atmospheric Component Of The MPI-M Earth System Model: ECHAM6, Journal of Advances in Modeling Earth Systems, 5, 146–172, https://doi.org/10.1002/jame.20015, 2013.

Taylor, K. E., Williamson, D., and Zwiers, F.: The sea surface temperature and sea-ice concentration boundary conditions for AMIP II simulations, Tech. Rep. 60, Program for Climate Model Diagnosis and Intercomparison, Lawrence Livermore National Laboratory, University
30   of California, 2000.

Timmermann, A., Oberhuber, J., Bacher, A., Esch, M., Latif, M., and Roeckner, E.: Increased El Niño Frequency In A Climate Model Forced By Future Greenhouse Warming, Nature, 398, 694–697, https://doi.org/10.1038/19505, 1999.

Tippett, M. K. and Giannini, A.: Potentially Predictable Components Of African Summer Rainfall In An SST-forced GCM Simulation, Journal of climate, 19, 3133–3144, https://doi.org/10.1175/JCLI3779.1, 2006.

35 Trenberth, K. E., Fasullo, J. T., and Mackaro, J.: Atmospheric Moisture Transports From Ocean To Land And Global Energy Flows In Reanalyses, Journal of Climate, 24, 4907–4924, https://doi.org/10.1175/2011jcli4171.1, 2011.

Wang, G. and Hendon, H. H.: Sensitivity Of Australian Rainfall To Inter-El Niño Variations, Journal of climate, 20, 4211–4226, https://doi.org/10.1175/JCLI4228.1, 2007.

Warman, L. and Moles, A. T.: Alternative stable states in Australia's Wet Tropics: a theoretical framework for the field data and a field-case for the theory, Landscape Ecology, 24, 1–13, https://doi.org/10.1007/s10980-008-9285-9, 2009.

Watson, J. E., Evans, T., Venter, O., Williams, B., Tulloch, A., Stewart, C., Thompson, I., Ray, J. C., Murray, K., Salazar, A., et al.: The Exceptional Value Of Intact Forest Ecosystems, Nature ecology & evolution, 2, 599–610, https://doi.org/10.1038/s41559-018-0490-x, 2018.

Wu, Z., Boke-Olén, N., Fensholt, R., Ardö, J., Eklundh, L., and Lehsten, V.: Effect of climate dataset selection on simulations of terrestrial GPP: Highest uncertainty for tropical regions, PloS one, 13, e0199 383, 2018.

Yang, K., Koike, T., Fujii, H., Tamagawa, K., and Hirose, N.: Improvement of Surface Flux Parametrizations With A Turbulence-Related Length, Quarterly Journal of the Royal Meteorological Society, 128, 2073–2087, https://doi.org/10.1256/003590002320603548, 2002.

Yeh, S.-W., Cai, W., Min, S.-K., McPhaden, M. J., Dommenget, D., Dewitte, B., Collins, M., Ashok, K., An, S.-I., Yim, B.-Y., et al.: ENSO Atmospheric Teleconnections And Their Response To Greenhouse Gas Forcing, Reviews of Geophysics, pp. 185–206, https://doi.org/10.1002/2017RG000568, 2018.

Zebiak, S. E., Orlove, B., Muñoz, Á. G., Vaughan, C., Hansen, J., Troy, T., Thomson, M. C., Lustig, A., and Garvin, S.: Investigating El Niño-Southern Oscillation And Society Relationships, Wiley Interdisciplinary Reviews: Climate Change, 6, 17–34, https://doi.org/10.7916/D84X577H, 2015.

Zemp, D. C., Schleussner, C.-F., Barbosa, H. M., Hirota, M., Montade, V., Sampaio, G., Staal, A., Wang-Erlandsson, L., and Rammig, A.: Self-amplified Amazon Forest Loss Due To Vegetation-Atmosphere Feedbacks, Nature communications, 8, 14 681, https://doi.org/10.1038/ncomms14681, 2017.

Zeng, N. and Neelin, J. D.: The Role Of Vegetation-Climate Interaction And Interannual Variability In Shaping The African Savanna, Journal of Climate, 13, 2665–2670, https://doi.org/10.1175/1520-0442(2000)013<2665:TROVCI>2.0.CO;2, 2000.

Zeng, N. and Yoon, J.: Expansion Of The World's Deserts Due To Vegetation-Albedo Feedback Under Global Warming, Geophysical Research Letters, 36, L17 401, https://doi.org/10.1029/2009GL039699, 2009.

Zhao, M., Heinsch, F. A., Nemani, R. R., and Running, S. W.: ImprovementS Of The MODIS Terrestrial Gross And Net Primary Production Global Data Set, Remote Sensing of Environment, 95, 164–176, https://doi.org/10.1016/j.rse.2004.12.011, 2005.

Zhou, C. and Wang, K.: Evaluation Of Surface Fluxes In ERA-Interim Using Flux Tower Data, Journal of Climate, 29, 1573–1582, https://doi.org/10.1175/JCLI-D-15-0523.1, 2016.